The Astrophysical Journal, 864:112 (9pp), 2018 September 10 https://doi.org/10.3847/1538-4357/aad23f
© 2018. The American Astronomical Society.
OPEN ACCESS

A Comparison of Alpha Particle and Proton Beam Differential Flows in Collisionally Young Solar Wind

B. L. Alterman[1,2], Justin C. Kasper[2,3], Michael L. Stevens[3], and Andriy Koval[4,5]
[1] University of Michigan, Department of Applied Physics, 450 Church Street, Ann Arbor, MI 48109, USA; balterma@umich.edu
[2] University of Michigan, Department of Climate & Space Sciences & Engineering, 2455 Hayward Street, Ann Arbor, MI 48109-2143, USA
[3] Smithsonian Astrophysical Observatory Observatory, Building E, 60 Garden Street, Cambridge, MA 02138, USA
[4] Goddard Planetary Heliophysics Institute, University of Maryland Baltimore County, Baltimore, MD 21228, USA
[5] Heliospheric Physics Laboratory, NASA Goddard Space Flight Center, Greenbelt, MD 20771, USA
Received 2018 April 5; revised 2018 July 6; accepted 2018 July 6; published 2018 September 5

Abstract

In fast wind or when the local Coulomb collision frequency is low, observations show that solar wind minor ions and ion subpopulations flow with different bulk velocities. Measurements indicate that the drift speed of both alpha particles and proton beams with respect to the bulk or core protons rarely exceeds the local Alfvén speed, suggesting that a magnetic instability or other wave–particle processes limits their maximum drift. We compare simultaneous alpha particle, proton beam, and proton core observations from instruments on the *Wind* spacecraft spanning over 20 years. In nearly collisionless solar wind, we find that the normalized alpha particle drift speed is slower than the normalized proton beam speed, no correlation between fluctuations in both species' drifts about their means, and a strong anti-correlation between collisional age and alpha–proton differential flow, but no such correlation with proton beam–core differential flow. Controlling for the collisional dependence, both species' normalized drifts exhibit similar statistical distributions. In the asymptotic, zero Coulomb collision limit, the youngest measured differential flows most strongly correlate with an approximation of the Alfvén speed that includes proton pressure anisotropy. In this limit and with this most precise representation, alpha particles drift at 67% and proton beam drift is approximately 105% of the local Alfvén speed. We posit that one of two physical explanations is possible. Either (1) an Alfvénic process preferentially accelerates or sustains proton beams and not alphas or (2) alpha particles are more susceptible to either an instability or Coulomb drag than proton beams.

Key words: plasmas – magnetohydrodynamics (MHD) – solar wind – waves

1. Introduction

Simple models of solar wind acceleration (e.g., Parker 1958) are unable to explain the solar wind's acceleration to high speeds. Wave–particle interactions are likely necessary to explain these observations. Differential flow is one useful indicator of such interactions and related acceleration.

Ionized hydrogen (protons) is the most common ion in the solar wind, usually constituting over 95% by number density. Within a few thermal widths of their mean speed, solar wind protons are well described by a single bi-Maxwellian velocity distribution function (VDF). However, an asymmetric velocity space shoulder has also been observed in the proton distribution. It can be described by a second, differentially flowing Maxwellian. We refer to the primary proton component as the proton core (p_1) and the secondary component as the proton beam (p_2). Proton beams are most easily measured in fast solar wind or when the local Coulomb collision frequency is small in comparison to the local expansion time. Fully ionized helium (alpha particles, α) is the second most common species and constitutes ∼4% of the solar wind by number density.

Differential flow is the velocity difference between two ion species or populations. It has been measured in the solar wind plasma at many solar distances starting in the corona and, when the local collision rate is smaller than the expansion time, extending out to and beyond 1 au (Feldman et al. 1974; Asbridge et al. 1976; Neugebauer 1976; Marsch et al. 1982a, 1982b; Goldstein et al. 1995; Steinberg et al. 1996; Kasper et al. 2008; Landi & Cranmer 2009). Kasper et al. (2006) showed that α differential flow is aligned with the magnetic field $\boldsymbol{B}$ to within several degrees as long as it is larger than ∼1% of the measured solar wind speed, i.e. any nonparallel flow is a measurement error. It should not be surprising that differential flow is field aligned because any finite differential flow perpendicular to $\boldsymbol{B}$ would immediately experience a Lorentz force until the plasma was again gyrotropic on a timescale comparable to the ion gyroperiod. We denote differential flow as $\Delta v_{b,c} = (\boldsymbol{v}_b - \boldsymbol{v}_c) \cdot \hat{\boldsymbol{b}}$, where ion species b differentially streams with respect to core population c and $\hat{\boldsymbol{b}}$ is the magnetic field unit vector. Positive differential flow is parallel to local $\boldsymbol{B}$ and negative differential flow is antiparallel to it. Simultaneous measurements of α-particles and protons indicate that $\Delta v_{\alpha,p1}$ is typically $\lesssim$70% of the local Alfvén speed, C_A (Feldman et al. 1974; Asbridge et al. 1976; Neugebauer 1976; Kasper et al. 2008, 2017). Simulations by Maneva et al. (2015) showed that a nonlinear streaming instability limits alpha particle drift to a maximum of 0.5 C_A. While measurements of heavier ions (e.g., iron, oxygen, carbon) show similar behavior (Berger et al. 2011), proton beam–core differential flow ($\Delta v_{p_2,p_1}$) has been reported at approximately the local Alfvén speed or larger (Marsch et al. 1982b). Given that the local Alfvén speed in the solar wind is generally a decreasing function of distance from the Sun, this apparent Alfvén speed limit implies that there is a local wave-mitigated limit on $\Delta v_{p2,p1}$, for which several

Original content from this work may be used under the terms of the Creative Commons Attribution 3.0 licence. Any further distribution of this work must maintain attribution to the author(s) and the title of the work, journal citation and DOI.

instability processes have been hypothesized (Daughton & Gary 1998; Daughton et al. 1999; Goldstein et al. 2000).

Raw data from the *Wind*/SWE Faraday cups are now archived at the NASA Space Physics Data Facility (SPDF) and are available online at CDAweb. We have developed a new fitting algorithm that returns simultaneous parameters for three solar wind ion populations (α, p_1, and p_2) and have processed over 20 years for Faraday cup solar wind measurements. For this project, we have restricted the analysis to measurements with clear differential flow signatures for both the alpha particle and proton beam components. We find that $\Delta v_{\alpha,p_1}/C_A$ and $\Delta v_{p_2,p_1}/C_A$ are indeed clustered around characteristic values that are consistent with previous results, but with considerable spreads in the respective distributions. We investigate possible contributions to the spreads, the apparent impact of Coulomb collisions in the weakly collisional regime, and the limitations of calculating the Alfvén speed under the commonly assumed frameworks of ideal and anisotropic MHD. We report that in collisionless solar wind:

1. α particle and p_2 differential flow speeds exhibit distinctly different trends with the locally measured Coulomb collision rate;
2. Coulomb collisions account for the dominant contribution to the spread in $\Delta v/C_A$; and
3. an accounting for the proton pressure anisotropy in the local Alfvén speed, as under anisotropic MHD, significantly reduces the spread in $\Delta v/C_A$.

For the most nearly collisionless solar wind measured at 1 au and using the more precise, anisotropic approximation of the Alfvén speed we report that

1. $\Delta v_{p_2,p_1}$ is 106% ± 15% of the local Alfvén speed,
2. $\Delta v_{\alpha,p_1}$ is 62% ± 13% of the local Alfvén speed, and
3. $\Delta v_{p_2,p_1} \approx 1.7 \times \Delta v_{\alpha,p_1}$.

Finally, we extrapolate to the perfectly collisionless limit, and estimate that

1. $\Delta v_{p_2,p_1}$ is ∼105% ± 15% of the Alfvén speed, and
2. $\Delta v_{\alpha,p_1}$ is 67% ± 9% of the Alfvén speed.

2. Data Sources and Selection

The *Wind* spacecraft launched in the fall of 1994. Its twin Faraday cup instruments have collected over 6.1 million proton and alpha particle direction-dependent energy spectra, the majority of which are in the solar wind (Ogilvie et al. 1995). These raw spectra consist of measured charge flux as a function of angle and energy-per-charge for each cup. With these spectra, we reconstruct 3D VDFs for each ion species and extract the bulk plasma properties: number density, velocity, and thermal speed. Over more than 20 years, refinements in the data processing algorithms have yielded new information from these distributions including precise α-particle abundances (Aellig et al. 2001; Kasper et al. 2007, 2012), perpendicular to parallel proton temperature ratios (Kasper et al. 2002, 2008), and relative alpha to proton temperature ratios (Kasper et al. 2008; Maruca et al. 2013).

Ogilvie et al. (1995) provide a thorough description of the Solar Wind Experiment (SWE). In summary, the SWE Faraday cups measure a single energy window approximately every 3 s and a full spectrum combines multiple energy windows measured over ∼92 s. Our fitting algorithm utilizes magnetic field measurements from the *Wind* Magnetic Field Investigation (MFI; Lepping et al. 1995; Koval & Szabo 2013) to determine each VDF's orientation relative to the local magnetic field and it assumes that the extracted parameters are approximately constant over the measurement time. In spectra for which this is not the case, automatically processed bulk properties can be unreliable.

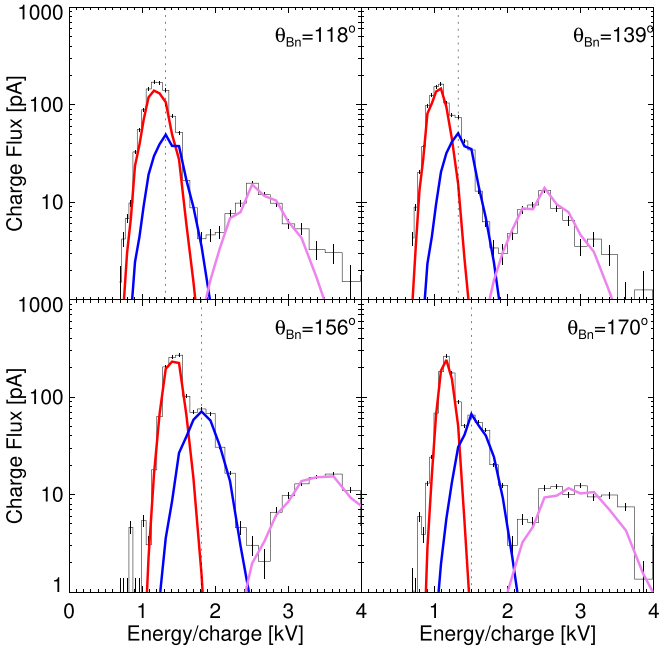


Figure 1. Fits from four example look directions from the *Wind* Faraday cups using a new data processing algorithm. Three ion populations are shown: α (purple), p_1 (red), and p_2 (blue). The angle of a given look direction with respect to the average magnetic field throughout the spectrum is indicated at the top right of each panel. Errors for each energy/charge bin are vertical dashed lines.

This new fitting algorithm returns 15 simultaneous parameters for three solar wind ion populations: alpha particles (α), proton cores (p_1), and proton beams (p_2). Kasper et al. (2006) describe the six-parameter α fitting routines. The protons are jointly fit by a nine-parameter set: six to p_1 (number density, vector velocity, and parallel and perpendicular temperature) and three to p_2 (number density, differential flow, and isotropic thermal speed).

Previous work with this data includes studies by Chen et al. (2016) and Gary et al. (2016). Figure 1 shows example energy-per-charge measurements made in four representative look directions. These directions are identified by the angle between the magnetic field and the direction normal to the Faraday cup's aperture. Figure 2 provides the corresponding proton (top) and α (bottom) VDFs. The proton beam is the extension of the proton VDF to large $v_{\parallel} > 0$.

Our alpha particle and proton core quality requirements nominally follow Kasper et al. (2002, 2007, 2008). Because this study focuses on measurements with a clear differential flow signature, we allow an additional class of fits for which the alpha particle temperature has been fixed to the proton core temperature so long as the alphas are well separated from the proton beam. To ensure that the magnetic field is suitably constant over the measurement time, we follow Kasper et al. (2002) and we reject spectra for which the rms fluctuation of

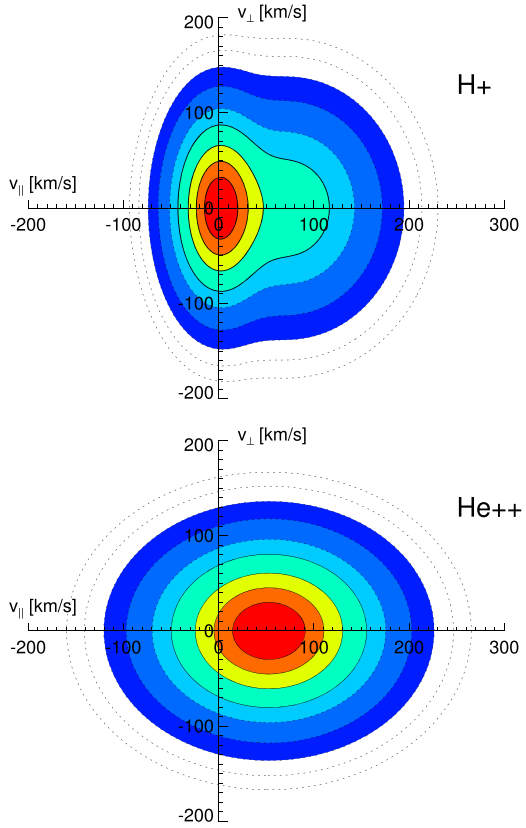


Figure 2. VDFs corresponding to the spectrum shown in Figure 1. The joint proton VDF (top) and α-particle VDF (bottom) are shown. The proton beam can be identified by the secondary shoulder at large $v_{\parallel}$ in the top panel. Contours follow Marsch et al. (1982b). In decreasing order, solid lines are 0.8, 0.6, 0.4, and 0.2 and dashed lines are 0.1, 0.032, 0.01, 0.0031, and 0.001 of the maximum phase-space density.

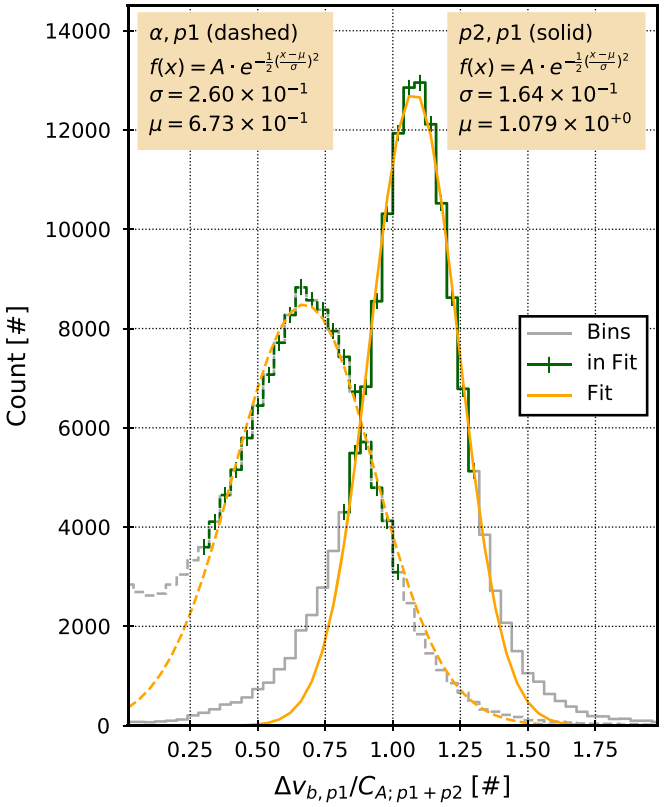


Figure 3. Normalized alpha particle (α, p_1) and proton beam (p_2, p_1) differential flows in collisionless, fast solar wind. Both differential flows are normalized by an Alfvén speed approximation from Equation (2) using both proton densities. Bins within 30% of the maximum are selected for fitting to exclude core–halo distributions.

the local magnetic field direction is larger than 20°. In addition to the reported impact on alpha particle measurements, we find that excluding these spectra also improves the overall quality of reported proton beams. To ensure that the beam is well constrained, we only include spectra for which the beam phase-space density is larger than the core phase-space density at the beam's bulk velocity, i.e., $f_{p_2}/f_{p_1}(\boldsymbol{v}_{p_2}) \geqslant 1$. The vertical dashed lines in Figure 1 indicate where this ratio is evaluated in each look direction. The look directions that are most aligned with the magnetic field direction give the clearest view of the beam.

3. Fast Wind Differential Flow

Figure 3 shows the distributions of simultaneously measured differential flows in the fast wind ($v_{\rm sw} \geqslant 400$ km s^{-1}) under conditions where the alphas and protons are both roughly collisionless ($10^{-2} \lesssim A_c \lesssim 10^{-1}$).[6] The dashed lines are alpha–proton core differential flow ($\Delta v_{\alpha,p_1}/C_A$) and the solid lines are proton beam–core differential flow ($\Delta v_{p_2,p_1}/C_A$). Here, we normalize to the ideal MHD Alfvén speed following Equation (2) and consider only the proton beam and core densities.[7] The gray lines are histograms of all data. In order to extract representative values and spreads thereof, we fit the green regions corresponding to 30% of the peak with a Gaussian. In selecting this portion of the histogram, we implicitly exclude an allowed class of proton VDF fits in which dominant non-Maxwellian features appear as large tails or a halo in the proton distribution instead of a secondary peak or shoulder-like fit because the uncertainty on the drift velocity is large. We leave these core–halo distributions for a later study. For the α-particle case, there is a distinct population with small drifts resulting from a combination of noise and poor-quality fits. Requiring $\Delta v_{\alpha,p1}/C_A \geqslant 0.27$ addresses this issue. The best-fit Gaussians are shown in orange. Similar to previous results (e.g., Marsch et al. 1982a; Reisenfeld et al. 2001; Kasper et al. 2008, 2017), $\Delta v_{\alpha,p_1}/C_A = 67\% \pm 26\%$ and $\Delta v_{p_2,p_1}/C_A = 108\% \pm 16\%$, where the ranges quoted are the 1σ widths of these fits. The widths of the Gaussians, which we will heretofore denote σ_{α,p_1} and σ_{p_2,p_1}, are attributed to a combination of (1) the range of measured solar wind conditions that support a nonzero differential flow and (2) applicable measurement errors. In the following sections, we hypothesize and test some potential contributions to each.

4. Uncorrelated Fluctuations

Differential flow is strongest in solar wind with large Alfvénic fluctuations and is therefore thought to be a signature of local wave–particle interactions, e.g., cyclotron-resonance-induced phase-space diffusion for the case of proton beaming (Tu et al. 2004). If differential flow is in general a product of local wave–particle interactions, the difference in widths observed in the Figure 3 histogram may follow from a resonance condition or aspect of the wave–particle coupling that depends on ion species characteristics, such as charge-to-mass ratio. To test this,

[6] See Section 5 for a discussion of collisional age.
[7] See Section 6 for a discussion of the Alfvén speed.

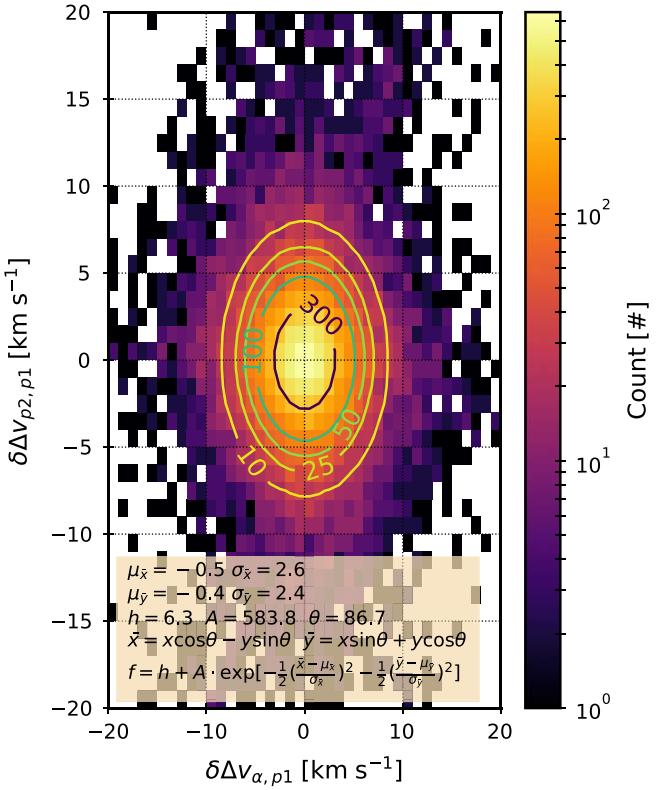


Figure 4. 2D histogram showing uncorrelated differential flow fluctuations ($\delta\Delta v$) for $\Delta v_{\alpha,p_1}$ and $\Delta v_{p_2,p_1}$. That the fit is a circle centered on the origin indicates that the fluctuations are uncorrelated.

we compare the magnitudes of correlated α and p_2 streaming fluctuations about their mean.

Figure 4 is a 2D histogram of proton beam differential flow fluctuations ($\delta\Delta v_{p_2,p_1}$) and alpha differential flow fluctuations ($\delta\Delta v_{\alpha,p_1}$), each about their mean. Comparing fluctuations in Δv removes other sources of variation in the magnitude of Δv, such as large-scale variations in the Alfvén speed or the bulk speed of the solar wind. Fluctuations are calculated by subtracting a running 14 minute mean from each Δv time series and requiring spectra for ∼50% of the time period. Because the fitting algorithm returns the parallel component of the beam differential flow, comparing any other component would incorporate additional information about the magnetic field. An ellipse is fit to the 2D histogram; contours of the fit are shown. The insert gives the function and fit parameters. The ellipse is a circle centered at the origin, indicating that the variations in $\Delta v_{\alpha,p_1}$ and $\Delta v_{p_2,p_1}$ are uncorrelated on these scales. We conclude that the difference in Δv distribution widths, i.e., $\sigma_{\alpha,p_1} \neq \sigma_{p_2,p_1}$, described in the previous section is not due to any species-specific difference in response to large-scale, local fluctuations. We repeated this calculation for running means calculated over various time intervals ranging from 5 minutes to more than 20 minutes and multiple requirements for the minimum number of spectra per window. The result is not sensitive to either parameter.

5. Trends with Collisional Age

In a hot and tenuous plasma—even in the absence of classical hard collisions—the cumulative effect of small angle Coulomb collisions acts like a simple drag force that gradually slows differentially flowing particles (Spitzer 1962). Tracy et al. (2016) showed that collisions with bulk protons are the dominant source of Coulomb drag on all other ions in the solar wind. The Coulomb collisional age is the ratio of the local collision rate to the local expansion time. Kasper et al. (2008, 2017) have demonstrated that $\Delta v_{\alpha,\mathrm{p1}}/C_\mathrm{A}$ is a strong exponentially decaying function of it.

The differential equation describing Coulomb drag is $\frac{d\Delta v}{dt} = -\nu_c \Delta v$, where ν_c is the effective collision rate. In integral form, this becomes $\Delta v = \Delta v_0 \exp\left[-\int_0^{t_0} \nu_c dt\right]$. Under the highly simplified assumption that ν_c and the solar wind speed (v_sw) are constant over the propagation distance r, the integral is commonly estimated as $\int_0^{t_0} \nu_c dt = \nu_c r/v_\mathrm{sw}$. We follow Kasper et al. (2008) and refer to this empirical proxy for the total number of collisions experienced over the expansion history as the collisional age (A_c) of the solar wind:

$$A_c = \nu_c \times \frac{r}{v_\mathrm{sw}}. \quad (1)$$

Kasper et al. (2017) refer to the same quantity as the Coulomb number (N_c). Chhiber et al. (2016) provide a detailed comparison of this empirical proxy to simulations. As we show below, the exponential decay of Δv with collisional age implies that $\Delta v\,/C_A$ histogram widths σ_{α,p_1} and σ_{p_2,p_1} are highly sensitive to the range of A_c in the sample.

Based on the work of Tracy et al. (2016), we neglect collisions among the minor populations themselves and only consider collisions of α or p_2 ions with proton core ions (p_1). Based on the work of Kasper et al. (2008, 2017), we limit our analysis of the collisional age dependence to collisionless and weakly collisional regimes that constitute the range $10^{-2} \lesssim A_c \lesssim 10^{-1}$. This is the range in which $\Delta v_{\alpha,p_1}/C_A$ is empirically nonzero.

Because the proton beam can have a non negligible density in comparison to the proton core, we calculate the collision frequency between two species following Hernaández & Marsch (1985, Equation (23)) in a self-consistent manner by integrating over test and field particles from both components. Our treatment of the Coulomb logarithm follows Fundamenski & Garcia (2007, Equation (18)). We assume that r is the distance traveled from a solar source surface to the spacecraft's radial location, ≈1 au, and we take the solar wind velocity to be $v_\mathrm{sw} \approx v_{p_1}$.

Measurements of $\Delta v_{\alpha,p_1}/C_A$ and $\Delta v_{p_2,p_1}/C_A$ are binned by collisional age and histogrammed in Figure 5 across the aforementioned range. Each column has been normalized by its maximum value in order to emphasize the trends with A_c. Only bins with at least 30% of the column maximum are shown. To characterize the collisionally "youngest" solar wind spectra that have been measured, we define a sufficiently large and statistically significant subset that reflects the limiting behavior. We have chosen this "youngest" range to be $10^{-2} \leqslant A_c \leqslant 1.2 \times 10^{-2}$. The rightmost limit of this subset is marked with a blue line on the figure.

In the case of α particles, the decrease from the mean value in the reference or youngest region of $\Delta v_{\alpha,p_1}/C_A \sim 0.8$ down to $\Delta v_{\alpha,p_1}/C_A \sim 0.4$ over the range shown would appear to account for a significant fraction of σ_{α,p_1}, up to a ∼40% spread. In contrast, the proton beam analog exhibits a far weaker apparent decay with increasing collisions, showing a decrease of at most approximately one-tenth the slope of the alpha particle trend.

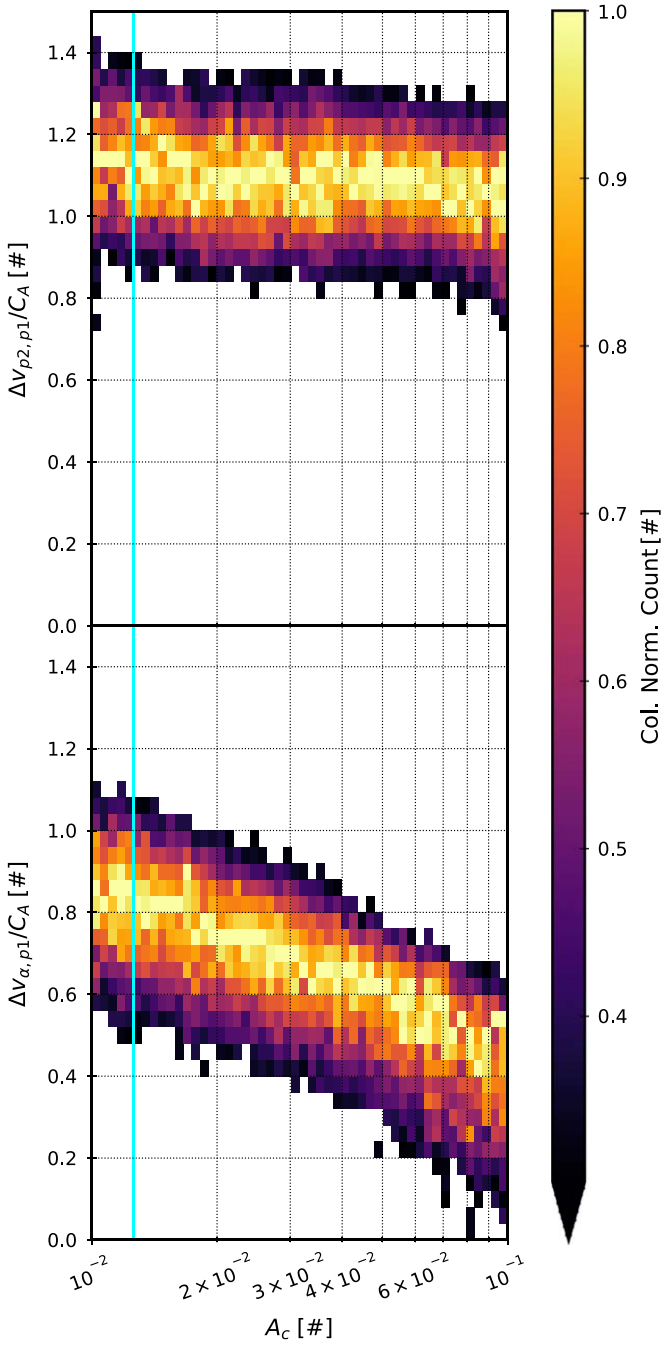


Figure 5. 2D histograms of α-particle and p_2 Alfvén speed normalized differential flows, each as a function of its collisional age. Only bins with at least 30% of the a column maximum are shown. Measurements with a collisional age $A_c \lesssim 1.2 \times 10^{-2}$ are indicated to the left of the blue line.

In other words, $\Delta v_{p_2,p_1}/C_A$ is nearly independent of the collisional age.

We would also like to derive the general and limiting cases for the differential flow speed ratios $\Delta v_{p2,p1}/\Delta v_{\alpha,p1}$ in spectra where the two are observed simultaneously. In Figure 6, we compare $\Delta v_{\alpha,p_1}$ to $\Delta v_{p_2,p_1}$ directly in the full low-collision regime and in the very young reference regime. The ratios $\Delta v_{\alpha,p_1}/\Delta v_{p_2,p_1}$ are histogrammed, with the dashed line indicating the full low-collision sample $10^{-2} \leqslant A_c \leqslant 10^{-1}$ and the solid line indicating the reference or youngest subsample $10^{-2} \leqslant A_c \leqslant 1.2 \times 10^{-2}$. The selection of data that contributes to Figure 6 is slightly different and more restrictive than

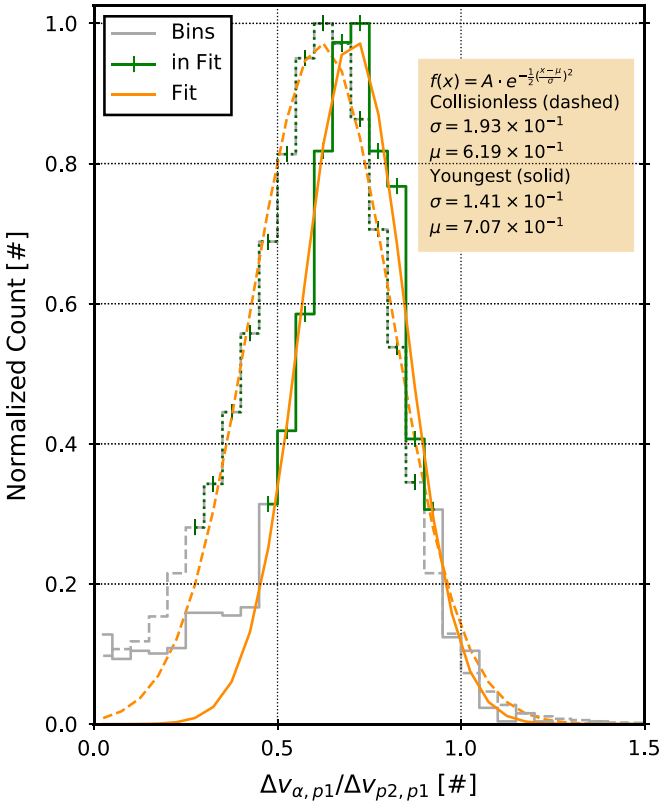


Figure 6. Ratio of alpha particle to proton beam differential flow ($\Delta v_{\alpha,p_1}/\Delta v_{p_2,p_1}$) in collisionless ($10^{-2} \leqslant A_c \leqslant 10^{-1}$; dashed) and the youngest measured ($10^{-2} \leqslant A_c \leqslant 1.2 \times 10^{-2}$; solid) data.

in the previous section, because here we require that both the alpha–core and proton beam–core collision rates simultaneously fall in the target range.

As before, we characterize these distributions in Figure 6 in a manner insensitive to the tails by fitting a Gaussian to bins with a count of at least 30% of the most populated bin. Similar to Figure 3, all binned data are shown in gray, the regions fit are green, and the fits are orange. The text inserts give the functional form and fit parameters up to the fit uncertainty. As there are fewer counts in the youngest A_c range, the histograms have been normalized by their maximum values in order to emphasize the difference in the respective means (μ) and widths (σ) of the distributions.

Over the low-collision range, $\Delta v_{p_2,p_1}$ is approximately 1.6× faster than $\Delta v_{\alpha,p_1}$. Over the youngest range, that reduces to 1.4×. The width or characteristic spread in $\Delta v_{\alpha,p_1}/\Delta v_{p_2,p_1}$ is 1.37× larger over the broader, low-collision range than the youngest range. Having demonstrated that $\Delta v_{\alpha,p_1}$ and $\Delta v_{p_2,p_1}$ are uncorrelated in these ranges and that the mean value of $\Delta v_{\alpha,p_1}/C_A$ changes by about 0.4 over the full range, we attribute most of the spread in the ratio $\Delta v_{\alpha,p_1}/\Delta v_{p_2,p_1}$ to the observed decay of $\Delta v_{\alpha,p_1}$ with increasing Coulomb collisions.

6. Corrections to the Alfvén Speed

Alfvén waves are parallel-propagating, transverse, noncompressive fluctuations in MHD plasmas (Alfvén 1942). Under ideal MHD and considering only a single, simple fluid, the phase speed of these waves (the Alfvén speed) is given by the ratio of the magnetic field magnitude (B) to the square root

Table 1
All Fit Parameters and Their Uncertainties in the Manner Calculated in Figure 7

Wave Speed Normalization	Alpha Particle		Proton Beam	
	Mean	Width	Mean	Width
$C_{A;\alpha+p1+p2}^{(\mathrm{Ani})}$	0.869	0.177	1.167	0.169
$C_{A;\alpha+p1+p2}^{(\mathrm{Ani})}$ $(p_{\tilde{v}})$	0.999	0.244	1.339	0.256
$C_{A;\alpha+p1}^{(\mathrm{Ani})}$	0.730	0.142	0.997	0.156
$C_{A;\alpha+p1}^{(\mathrm{Ani})}$ $(p_{\tilde{v}})$	0.761	0.164	1.048	0.172
$C_{A;p1+p2}^{(\mathrm{Ani})\,*}$	0.784	0.160	**1.057**	**0.150**
$C_{A;p1+p2}^{(\mathrm{Ani})}$ $(p_{\tilde{v}})^*$	0.876	0.206	1.182	0.205
$C_{A;p1}^{(\mathrm{Ani})}$	**0.622**	**0.132**	0.874	0.164
$C_{A;\alpha+p1+p2}$	0.902	0.194	1.227	0.177
$C_{A;\alpha+p1}$	0.755	0.166	1.052	0.179
$C_{A;p1+p2}{}^*$	0.829	0.181	1.131	0.166
$C_{A;p1}$	0.657	0.150	0.938	0.183

Note. The columns indicate the parameter (mean value or width) for a given differentially flowing species. The rows indicate the wave speed normalization. The preferred normalizations are indicated in bold. Anisotropic Alfvén speeds including the dynamic pressure term from Equation (3) are indicated by $(p_{\tilde{v}})$. The average fit uncertainty on the mean is 4×10^{-3} and the average uncertainty on width is 5×10^{-3}. Normalizations marked with an asterisk (*) are plotted in Figure 8.

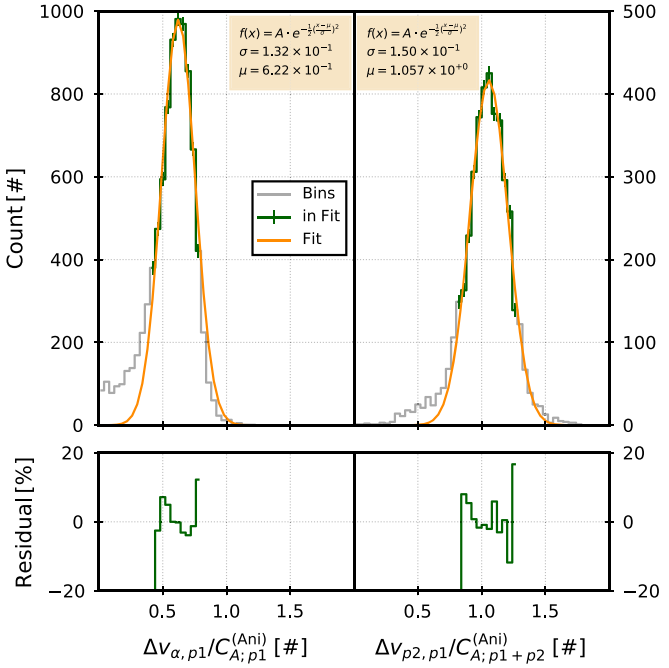


Figure 7. Examples of the Gaussian fits to 1D distributions of α and p_2 normalized differential flow along with the associated residuals. As discussed in Section 6, the Alvén speed normalizations shown minimize the width of these distributions.

of the mass density (ρ):

$$C_A = \frac{B}{\sqrt{\mu_0 \rho}}. \tag{2}$$

Barnes & Suffolk (1971) derived an approximation to the Alfvén speed under anisotropic MHD that accounts for pressure anisotropy and differential flow of multiple ion species:

$$C_A^{\mathrm{Ani}} = C_A\left[1 + \frac{\mu_0}{B^2}(p_\perp - p_\parallel) - \frac{\mu_0}{B^2}p_{\tilde{v}}\right]^{1/2}. \tag{3}$$

Here, C_A is the ideal MHD Alfvén speed from Equation (2). The second term in the brackets gives the correction due to the thermal anisotropy of the plasma. Total thermal pressure perpendicular and parallel to the local magnetic field are $p_i = \sum_s n_s k_b T_{s,i} = \frac{\rho_{p1}}{2}\sum_s \frac{\rho_s}{\rho_{p1}} w_{s;i}^2$ for components $i = \perp, \parallel$. The third term in the brackets gives the correction due to the dynamic pressure from differential streaming in the plasma frame, which is $p_{\tilde{v}} = \sum_s \rho_s (\boldsymbol{v}_s - \boldsymbol{u})^2 = \rho_{p_1}\sum_s \frac{\rho_s}{\rho_{p1}}(\boldsymbol{v}_s - \boldsymbol{u})^2$. Here, $\boldsymbol{u}$ is the plasma's center-of-mass velocity, a given species' mass density is ρ_s, and its velocity is $\boldsymbol{v}_s$. All species s are summed over. Pressure terms have been written in terms of mass density ratios to emphasize the significance of correction factors discussed in the following paragraphs and cataloged in Table 1. When the plasma is isotropic and there is either vanishingly slow differential flow or a vanishingly small differentially flowing population, the term in brackets is equal to unity and Equation (3) reduces to (2).

This anisotropic, multi-component formalism of Barnes & Suffolk (1971) ought to be a more appropriate and higher-fidelity description of the solar wind plasma than the commonly evoked ideal single-fluid approximation. Nevertheless, it is instructive to give a rough illustration of the magnitude of each correction term under typical conditions. We note first that the proton core in the solar wind is often anisotropic, with core pressure ratios falling primarily in the range $0.1 \lesssim p_\perp/p_\parallel \lesssim 10$. The absolute correction to the Alfvén speed, via the second bracketed term in Equation (3), that follows from this anisotropy alone is ~6%–7% for the median case and can be as high as ~50%. With regards to the third bracketed term, we note that a typical proton beam carrying 10% of the total protons at a speed of roughly C_A relative to the core would carry a ~5% self-consistent correction to the Alfvén speed, owing to proton beam–core dynamic pressure.

Our goal in this section is to relax the ideal MHD approximation by considering these next-order approximations for the speed of the predominant parallel-propagating wave in the solar wind. We explore whether the spreads in normalized differential flow, i.e., the widths of the 1D distributions of $\Delta v/C_A$, are further minimized when the contributions of anisotropic and dynamic pressure are considered. In order to disentangle this element from the Coulomb collision effect described in the previous section, we limit our analysis in this section to the "youngest" plasma, i.e., measurements drawn from the youngest measured reference regime to the left of the blue line in Figure 5.

Figure 7 plots distributions and fits in the now-familiar style, together with the fit residuals, for one possible renormalization of $\Delta v_{\alpha,p_1}/C_A$ and $\Delta v_{p_2,p_1}/C_A$. The color selection for the various components in the top panel follows the convention from the previous figures. Again, only bins with counts at least 30% of the maximum are used in the fit. Residuals are shown for the bins in the fit, and the fit parameters are shown in the inserts. The amplitudes A are omitted because they are of no consequence. In this particular case, the α and p_2 differential flow are normalized by the Alfvén speeds with proton core pressure anisotropy taken into account. For reasons discussed below, the normalization in the proton beam–core example

(right) also accounts for the beam contribution to the proton mass density.

We consider a family of similar approximations to the Alfvén speed, each accounting for corrections associated with the measured anisotropies and multiple component terms in Equation (3). As these contributions rely on higher-order moments of the spectrum fit,[8] they can carry relatively large uncertainties. If the uncertainties are significant in the aggregate, they are expected to contribute to broadening of the $\Delta v/C_A$ distributions. However, terms that are well measured in the aggregate will improve the precision of the Alfvén speed when accounted for and thus reduce the width of $\Delta v/C_A$ if the true differential flows are Alfvénic in nature. In the following, we examine all possible combinations in order to ascertain whether a well-measured high-order correction exists that further minimizes the width of the normalized differential flow distributions.

Table 1 contains fit parameters for each 1D distribution of $\Delta v/C_A$, for both the alpha–proton and proton beam–core differential flows, using the various formulations of the Alfvén speed. Overall, we find that the widths of both $\Delta v/C_A$ distributions increase substantially when the dynamic pressure term is included, indicating that either (1) the differential flows are *less* strongly correlated with anisotropic Alfvén speed in Equation (3), or (2) that the additional measurement uncertainty introduced along with a given term is in the aggregate comparable to the correction itself.

However, when only the proton core temperature anisotropy correction is factored in, the distribution width is indeed reduced relative to the isotropic case. Because the core anisotropy correction term in Equation (3) is usually (but not always) positive, it tends to increase the Alfvén speed estimate relative to the ideal MHD approximation. Thus, the corrected mean values $\Delta v/C_A$ are generally lower. Figure 8 is a plot of the width versus mean for select 1D fits that were performed in the style of Figure 7, illustrating these observations. In the cases shown, each Alfvén speed includes both proton densities. The cases accounting for proton core pressure anisotropy correction factor ($p_\perp - p_\parallel$) are indicated with the square. Cases that additionally account for the proton core dynamic pressure correction factor ($p_\perp - p_\parallel - p_{\tilde{v}}$) are indicated by stars.

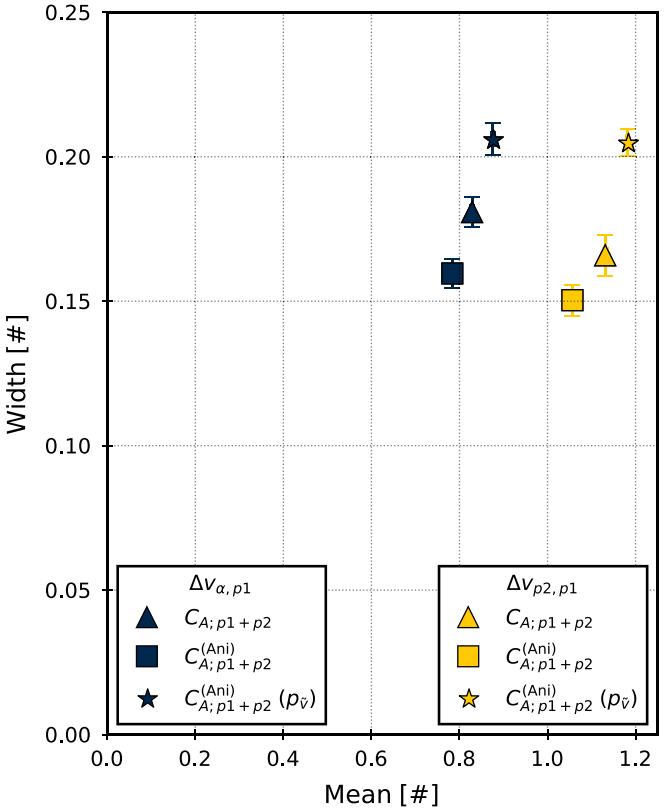


Figure 8. Example α-particle and p_2 normalized differential flow illustrating the impacts of various Alfvén speed approximations. In both cases shown, inclusion of the proton core anisotropy (Equation (3)) reduces the width in comparison to the isotropic MHD Alfén speed (Equation (2)), while including the anisotropy and the dynamic pressure ($p_{\tilde{v}}$) increases it.

7. Trends in A_c

Using the Alfvén speed approximation that minimizes the spread in normalized differential flow for alphas and beams, we examine the behavior of $\Delta v/C_A$ as a function of A_c and in the asymptotic limit of zero collisions. We applied the same methodology used to examine 1D distributions in the youngest A_c data to binned α, p_1 and p_2, p_1 differential flow spanning the low-collision range. Figure 9 plots these trends. Alpha particles are shown in blue and proton beams in yellow. Pluses indicate mean values derived from 1D fits. Error bars indicate the associated 1D widths. Fits to each trend are given as black dotted lines.

Four clear features are apparent pertaining to the mean values of both normalized differential flows and to their collisional trends. First, if we consider the asymptotic limit of zero Coulomb collisions and we account for the widths reported in Table 1, the alpha particles differentially stream at 67% of the local Alfvén speed and the proton beams stream at approximately the Alfvén speed. Second, that the fit constant c governing α, p_1 decay is greater than 1 indicates that our collisional age calculation oversimplifies our A_c by either underestimating r, underestimating ν_c, overestimating v_{sw}, or some combination of these. Kasper et al. (2017) examined detailed scalings and more accurate versions of A_c that may correct for some of these issues and can be a subject for future study. Third, even using the formulation of the Alfvén speed that yields the highest precision, the spread in alpha particle differential flow due to the change in mean value over the collisionless range is still ~0.3, which is the largest single contribution to the spread in $\Delta v/C_A$. Fourth, in the asymptotic absence of collisions, the proton beams differentially flow at very nearly (105% of) the Alfvén speed. Given the widths of the error bars in Figure 9, the difference between the youngest resolved $\Delta v_{p_2,p_1}$ and the asymptotic value could be due to the spread in our measurements.

8. Discussion

The evolution of solar wind VDFs is governed by an interplay between adiabatic expansion, Coulomb collisions, and wave–particle interactions. Collisional transport rates (Livi & Marsch 1986; Pezzi et al. 2016) and many types of wave–particle interactions (Verscharen et al. 2013a, 2013b; Verscharen & Chandran 2013) depend on the small-scale structure of the VDF, in particular the small-scale velocity space gradients. Because measurements indicate the presence of alpha–proton differential flow starting at the corona and extending out to and beyond 1 au, one can assume that nonzero differential flow is a

[8] See Section 2.

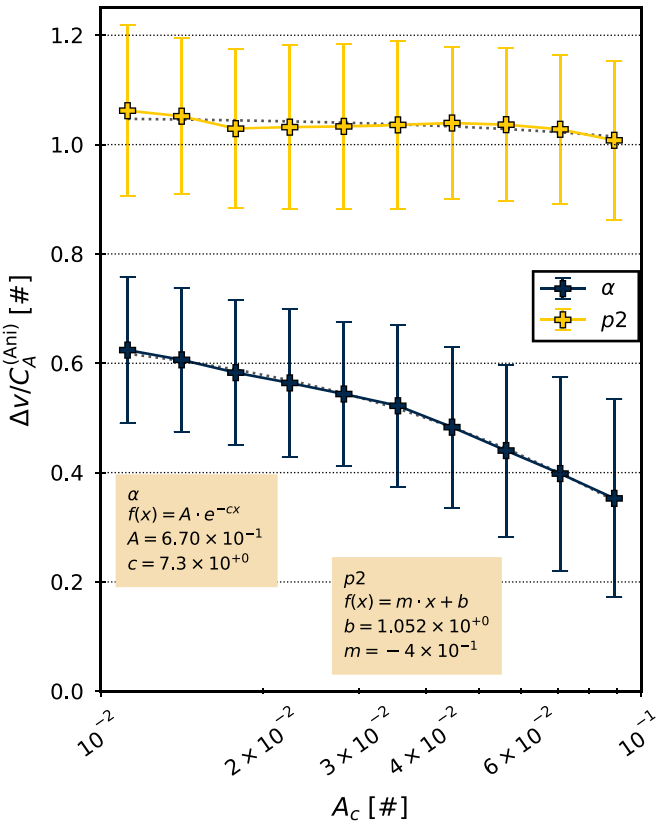


Figure 9. Trends of 1D fits to $\Delta v_{\alpha,p_1}/C_A$ and $\Delta v_{p_2,p_1}/C_A$ as a function of A_c. Error bars are the widths of the 1D fits. Each trend has been fit. The parameters are shown in the appropriate insert. While $\Delta v_{\alpha,p_1}$ markedly decays with increasing A_c, $\Delta v_{p_2,p_1}$ is relatively constant with A_c. To within the fit uncertainty, proton beams differentially stream at approximately the local Alfvén speed.

coronal signature. Under this hypothesis, the decay of $\Delta v_{\alpha,p1}$ is due to dynamical friction (Kasper et al. 2017). As the proton beam–core drift and alpha–core drift are signatures of one plasma with a single expansion history, the collisional bottleneck that erodes $\Delta v_{\alpha,p1}$ could likewise be expected to erode $\Delta v_{p2,p1}$. However, the observed independence of $\Delta v_{p2,p1}/C_A$ with respect to A_c over the examined range contradicts this assumption and minimally implies either (A) an additional competing process that preferentially couples to proton beams or (B) that Equation (1) underestimates the proton dynamical friction.

Several in situ mechanisms that preferentially couple to protons have been proposed. In the wave-particle case, Voitenko & Pierrard (2015) propose that the interaction between resonant protons and kinetic Alfvén waves leads to the local formation of beams. Such a mechanism could be responsible for the creation of proton beams throughout the solar wind's evolution or it could turn on at some distance from the Sun where plasma conditions become favorable. In the case of collisions, Livi & Marsch (1987) have argued that Coulomb scattering itself in the presence of the interplanetary magnetic field can produce skewed and beam-like distributions under certain circumstances.

The collisional age used in Equation (1) assumes that the collision frequency describing proton dynamical friction does not change over the solar wind's evolution and is equal to the value measured at the spacecraft. Chhiber et al. (2016) have shown that such assumptions do not capture the full nature of proton radial evolution. Equation (1) also neglects the ways in which this frequency depends on the small-scale structure of the VDF (Livi & Marsch 1986; Pezzi et al. 2016). One avenue of future work is to better address collisional effects by modeling the radial dependence, building on the work of Chhiber et al. (2016) and Kasper et al. (2017). A further refinement would be to account for dependence of collision frequency on the VDF fine structure (Livi & Marsch 1986; Pezzi et al. 2016). A second avenue of future work involves modeling the force required to locally maintain differential flow. By letting this force depend on local wave amplitudes, perhaps the differential flow radial evolution could be modeled from the competition between a Coulomb frictional force and a force from resonant scattering (Voitenko & Pierrard 2015).

The hypotheses of proton beams as coronal in origin or created and modified in situ are not mutually exclusive. For example, wave-resonant or frictional forcing may only be significant over a certain portion of the solar wind's radial evolution and that range may correspond to a subset of commonly measured conditions at 1 au. Applying a holistic model to data that is differentiated by wave power or Coulomb collisions may allow us to distinguish between or unite the two origin hypotheses. The upcoming Parker Solar Probe (Fox et al. 2015) and Solar Orbiter (Müller et al. 2013) missions, with their closer perihelia and higher energy resolution plasma instruments (Kasper et al. 2015), will also allow us to gauge the relative importance of and interplay between these effects.

9. Conclusions

In fast (>400 km s^{-1}) and collisionless ($A_c \leqslant 10^{-1}$) solar wind, α, $p1$ differential flow is approximately 62% as fast as $p2$, $p1$ differential flow when measured by the *Wind* spacecraft's Faraday cups. The spread in α, $p1$ differential flow is approximately 1.7× larger than $p2$, $p1$ differential flow. We ruled out large-scale, in-phase wave–particle interactions by examining the correlation between fluctuations in both species parallel differential flows over multiple timescales ranging from 5 minutes to more than 20 minutes. Minimizing the spread in normalized differential flow due to the method used to approximate the Alfvén speed, we found that the difference in $\Delta v/C_A$ width for both species is predominantly due to the decay of $\Delta v_{\alpha,p1}/C_A$ with increasing Coulomb collisions. At the youngest resolved collisional age, when the impact of Coulomb collisions has been minimized, we find that proton core pressure anisotropy has the largest impact on minimizing the spread in normalized differential flow and that the increase in spread when including dynamic pressure in the anisotropic Alfvén speed is beyond what would be expected from random fluctuations. In the asymptotic absence of Coulomb collisions, α-particles differentially flow at approximately 67% of the local Alfvén speed and proton beams differentially flow at approximately 105% of it. This upper limit on $\Delta v_{\alpha,p1}/C_A$ is close to the upper limit found by Maneva et al. (2014) and worth further investigation. We also found that, unlike the known (Neugebauer 1976; Kasper et al. 2008, 2017) $\Delta v_{\alpha,\mathrm{p1}}$ decay with A_c, proton beam differential flow minimally decays and is approximately constant with collisional age.

Given the results of Tracy et al. (2016) showing that solar wind ions collisionally couple most dominantly to protons, it is unsurprising that the widths of both $\Delta v_{\alpha,p1}/C_A$ and $\Delta v_{p2,p1}/C_A$ are smallest when the Alfvén speed accounts for the proton core. Chen et al. (2013) found that solar wind helicities are closer to unity when normalizing by the anisotropic Alfvén speed. That the proton core temperature anisotropy is significant in these results

further supports their conclusion. That the beam differential flow width is smaller when it is normalized by an Alfvén speed including the beam density may indicate some coupling between the beams and local Alfvén waves, as predicted by Voitenko & Pierrard (2015). That the dynamic pressure term causes a larger spread in both species normalized differential flow is either a result of measurement uncertainty or some underlying physical mechanism that is beyond the scope of this paper to test.

The authors thank K. G. Klein, D. Verscharen, and P. Whittlesey for useful discussions. B.L.A. and J.C.K. are supported by NASA grant NNX14AR78G. M.L.S. is supported by NASA grant NNX14AT26G. Both grants support *Wind* operations and data analysis.

Software: pandas (Mckinney 2010), Python (Millman & Aivazis 2011; Oliphant 2007), SciPy (Jones et al. 2001), NumPy (van der Walt et al. 2011), Matplotlib (Hunter 2007), IPython (Perez & Granger 2007), jupyter (Kluyver et al. 2016).

ORCID iDs

B. L. Alterman https://orcid.org/0000-0001-6673-3432
Justin C. Kasper https://orcid.org/0000-0002-7077-930X
Michael L. Stevens https://orcid.org/0000-0002-7728-0085

References

Aellig, M. R., Lazarus, A. J., & Steinberg, J. T. 2001, GeoRL, 28, 2767
Alfvén, H. 1942, Natur, 150, 405
Asbridge, J. R., Bame, S. J., Feldman, W. C., & Montgomery, M. D. 1976, JGR, 81, 2719
Barnes, A., & Suffolk, G. C. J. 1971, JPlPh, 5, 315
Berger, L., Wimmer-Schweingruber, R. F., & Gloeckler, G. 2011, PhRvL, 106, 151103
Chen, C. H. K., Bale, S. D., Salem, C. S., & Maruca, B. A. 2013, ApJ, 770, 125
Chen, C. H. K., Matteini, L., Schekochihin, A. A., et al. 2016, ApJL, 825, L26
Chhiber, R., Usmanov, A. V., Matthaeus, W. H., & Goldstein, M. L. 2016, ApJ, 821, 34
Daughton, W., & Gary, S. P. 1998, JGR, 103, 20613
Daughton, W., Gary, S. P., & Winske, D. 1999, JGR, 104, 4657
Feldman, W. C., Asbridge, J. R., & Bame, S. J. 1974, JGR, 79, 2319
Fox, N. J., Velli, M., Bale, S. D., et al. 2015, SSRv, 204, 7
Fundamenski, W., & Garcia, O. E. 2007, Comparison of Coulomb Collision Rates in the Plasma Physics and Magnetically Confined Fusion Literature, EUROfusion Tech. Rep. EFDA-JET-R(07)-01, http://www.euro-fusionscipub.org/archives/jet-archive/comparison-of-coulomb-collision-rates-in-the-plasma-physics-and-magnetically-confined-fusion-literature
Gary, S. P., Jian, L. K., Broiles, T. W., et al. 2016, JGRA, 121, 30
Goldstein, B. E., Neugebauer, M., & Smith, E. J. 1995, GeoRL, 22, 3389
Goldstein, B. E., Neugebauer, M., Zhang, L. D., & Gary, S. P. 2000, GeoRL, 27, 53
Hernández, R., & Marsch, E. 1985, JGR, 90, 11062
Hunter, J. D. 2007, CSE, 9, 90
Jones, E., Oliphant, T. E., & Peterson, P. 2001, SciPy: Open source scientific tools for Python, http://www.scipy.org/
Kasper, J. C., Abiad, R., Austin, G., et al. 2015, SSRv, 204, 131
Kasper, J. C., Klein, K. G., Weber, T., et al. 2017, ApJ, 849, 126
Kasper, J. C., Lazarus, A. J., & Gary, S. P. 2002, GeoRL, 29, 1839
Kasper, J. C., Lazarus, A. J., & Gary, S. P. 2008, PhRvL, 101, 261103
Kasper, J. C., Lazarus, A. J., Steinberg, J. T., Ogilvie, K. W., & Szabo, A. 2006, JGR, 111, A03105
Kasper, J. C., Stevens, M. L., Korreck, K. E., et al. 2012, ApJ, 745, 162
Kasper, J. C., Stevens, M. L., Lazarus, A. J., Steinberg, J. T., & Ogilvie, K. W. 2007, ApJ, 660, 901
Kluyver, T., Ragan-Kelley, B., Pérez, F., et al. 2016, in Positioning and Power in Academic Publishing: Players, Agents and Agendas, ed. F. Loizides & B. Schmidt (Amsterdam: IOS Press), 87
Koval, A., & Szabo, A. 2013, in AIP Conf. Proc. 1539, SOLAR WIND 13, ed. G. Zank et al. (Melville, NY: AIP), 211
Landi, E., & Cranmer, S. R. 2009, ApJ, 691, 794
Lepping, R. P., Acuna, M. H., Burlaga, L. F., et al. 1995, SSRv, 71, 207
Livi, S., & Marsch, E. 1986, AnGeo, 4, 333
Livi, S., & Marsch, E. 1987, JGR, 92, 7255
Maneva, Y. G., Araneda, J. A., & Marsch, E. 2014, ApJ, 783, 139
Maneva, Y. G., Ofman, L., & Viñas, A. 2015, A&A, 578, A85
Marsch, E., Mühlhäuser, K.-H., Rosenbauer, H., Schwenn, R., & Neubauer, F. M. 1982a, JGR, 87, 35
Marsch, E., Mühlhäuser, K.-H., Schwenn, R., et al. 1982b, JGR, 87, 52
Maruca, B. A., Bale, S. D., Sorriso-Valvo, L., Kasper, J. C., & Stevens, M. L. 2013, PhRvL, 111, 1
Mckinney, W. 2010, in Proc. 9th Python in Science Conf., ed. S. van der Walt & J. Millman, 51, http://conference.scipy.org/proceedings/scipy2010/mckinney.html
Millman, K. J., & Aivazis, M. 2011, CSE, 13, 9
Müller, D., Marsden, R. G., St., Cyr, O. C., & Gilbert, H. R. 2013, SoPh, 285, 25
Neugebauer, M. 1976, JGR, 81, 78
Ogilvie, K. W., Chornay, D. J., Fritzenreiter, R. J., et al. 1995, SSRv, 71, 55
Oliphant, T. E. 2007, CSE, 9, 10
Parker, E. N. 1958, ApJ, 128, 664
Perez, F., & Granger, B. E. 2007, CSE, 9, 21
Pezzi, O., Valentini, F., & Veltri, P. 2016, PhRvL, 116, 145001
Reisenfeld, D. B., Gary, S. P., Gosling, J. T., et al. 2001, JGR, 106, 5693
Spitzer, L. 1962, Interscience Tracts on Physics and Astronomy (2nd ed; New York: Interscience Publication)
Steinberg, J. T., Lazarus, A. J., Ogilvie, K. W., Lepping, R. P., & Byrnes, J. 1996, GeoRL, 23, 1183
Tracy, P. J., Kasper, J. C., Raines, J. M., et al. 2016, PhRvL, 116, 255101
Tu, C.-Y., Marsch, E., & Qin, Z. R. 2004, JGRA, 109, 5101
van der Walt, S., Colbert, S. C., & Varoquaux, G. 2011, CSE, 13, 22
Verscharen, D., Bourouaine, S., & Chandran, B. D. G. 2013a, ApJ, 773, 163
Verscharen, D., Bourouaine, S., Chandran, B. D. G., & Maruca, B. A. 2013b, ApJ, 773, 8
Verscharen, D., & Chandran, B. D. 2013, ApJ, 764, 88
Voitenko, Y., & Pierrard, V. 2015, SoPh, 290, 1231